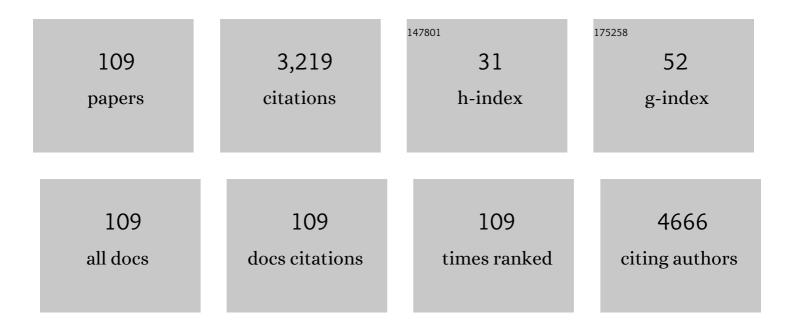


List of Publications by Year in descending order

Source: https://exaly.com/author-pdf/480471/publications.pdf Version: 2024-02-01



| # | Article | IF | CITATIONS |
|----|---|------|-----------|
| 1 | Wet Chemical Synthesis of Graphene. Advanced Materials, 2013, 25, 3583-3587. | 21.0 | 453 |
| 2 | Coordination and Metalation Bifunctionality of Cu with 5,10,15,20-Tetra(4-pyridyl)porphyrin: Toward a Mixed-Valence Two-Dimensional Coordination Network. Journal of the American Chemical Society, 2012, 134, 6401-6408. | 13.7 | 199 |
| 3 | Honeycomb-like Hard Carbon Derived from Pine Pollen as High-Performance Anode Material for Sodium-Ion Batteries. ACS Applied Materials & Interfaces, 2018, 10, 42796-42803. | 8.0 | 129 |
| 4 | Self-Assembly and Properties of Nonmetalated Tetraphenyl-Porphyrin on Metal Substrates. Journal of Physical Chemistry C, 2010, 114, 9408-9415. | 3.1 | 101 |
| 5 | Influence of surface chemistry on optical, chemical and electronic properties of blue luminescent carbon dots. Nanoscale, 2019, 11, 2056-2064. | 5.6 | 94 |
| 6 | Combined Photoemission and Scanning Tunneling Microscopy Study of the Surface-Assisted Ullmann Coupling Reaction. Journal of Physical Chemistry C, 2014, 118, 6820-6830. | 3.1 | 84 |
| 7 | Diffusion, Rotation, and Surface Chemical Bond of Individual 2 <i>H</i> -Tetraphenylporphyrin Molecules on Cu(111). Journal of Physical Chemistry C, 2011, 115, 24172-24177. | 3.1 | 74 |
| 8 | A high performance direct carbon solid oxide fuel cell – A green pathway for brown coal utilization. Applied Energy, 2019, 248, 679-687. | 10.1 | 74 |
| 9 | Temperature-Dependent Chemical and Structural Transformations from 2H-tetraphenylporphyrin to Copper(II)-Tetraphenylporphyrin on Cu(111). Journal of Physical Chemistry C, 2012, 116, 12275-12282. | 3.1 | 68 |
| 10 | Deactivation of nickel-based anode in solid oxide fuel cells operated on carbon-containing fuels. Journal of Power Sources, 2014, 268, 508-516. | 7.8 | 66 |
| 11 | Graphene/Substrate Charge Transfer Characterized by Inverse Photoelectron Spectroscopy. Journal of Physical Chemistry C, 2010, 114, 21618-21624. | 3.1 | 61 |
| 12 | Characterization of symmetrical SrFe0.75Mo0.25O3â^îr electrodes in direct carbon solid oxide fuel cells. Journal of Alloys and Compounds, 2016, 688, 939-945. | 5.5 | 61 |
| 13 | Surface state engineering of molecule–molecule interactions. Physical Chemistry Chemical Physics, 2012, 14, 4971. | 2.8 | 56 |
| 14 | Effective and environmentally friendly recycling process designed for LiCoO2 cathode powders of spent Li-ion batteries using mixture of mild organic acids. Waste Management, 2018, 78, 51-57. | 7.4 | 55 |
| 15 | Electrochemical gas–electricity cogeneration through direct carbon solid oxide fuel cells. Journal of Power Sources, 2015, 277, 1-8. | 7.8 | 52 |
| 16 | Evolution of Oxygen–Metal Electron Transfer and Metal Electronic States During Manganese Oxide Catalyzed Water Oxidation Revealed with Inâ€Situ Soft Xâ€Ray Spectroscopy. Angewandte Chemie - International Edition, 2019, 58, 3426-3432. | 13.8 | 52 |
| 17 | Abrupt Coverage-Induced Enhancement of the Self-Metalation of Tetraphenylporphyrin with Cu(111). Journal of Physical Chemistry C, 2014, 118, 1661-1667. | 3.1 | 51 |
| 18 | Electrolysis of Carbon Dioxide in a Solid Oxide Electrolyzer with Silver-Gadolinium-Doped Ceria Cathode. Journal of the Electrochemical Society, 2015, 162, F397-F402. | 2.9 | 47 |

| # | Article | IF | CITATIONS |
|----|---|------|-----------|
| 19 | A novel strategy for realizing high nitrogen doping in Fe ₃ C-embedded nitrogen and phosphorus-co-doped porous carbon nanowires: efficient oxygen reduction reaction catalysis in acidic electrolytes. Journal of Materials Chemistry A, 2019, 7, 17923-17936. | 10.3 | 47 |
| 20 | IrO2 nanoparticles highly dispersed on nitrogen-doped carbon nanotubes as an efficient cathode catalyst for high-performance Li-O2 batteries. Ceramics International, 2017, 43, 14082-14089. | 4.8 | 46 |
| 21 | Behavior of strontium- and magnesium-doped gallate electrolyte in direct carbon solid oxide fuel cells. Journal of Alloys and Compounds, 2014, 608, 272-277. | 5.5 | 40 |
| 22 | Unraveling the Electronic Structure of Photocatalytic Manganese Complexes by L-Edge X-ray Spectroscopy. Journal of Physical Chemistry C, 2015, 119, 19192-19200. | 3.1 | 40 |
| 23 | Effects of doping alumina on the electrical and sintering performances of yttrium-stabilized-zirconia. Solid State Ionics, 2016, 289, 28-34. | 2.7 | 40 |
| 24 | In Situ L-Edge XAS Study of a Manganese Oxide Water Oxidation Catalyst. Journal of Physical Chemistry C, 2017, 121, 12003-12009. | 3.1 | 40 |
| 25 | Enhanced electrokinetic remediation of lead- and cadmium-contaminated paddy soil by composite electrolyte of sodium chloride and citric acid. Journal of Soils and Sediments, 2018, 18, 1915-1924. | 3.0 | 40 |
| 26 | Joint Analysis of Radiative and Non-Radiative Electronic Relaxation Upon X-ray Irradiation of Transition Metal Aqueous Solutions. Scientific Reports, 2016, 6, 24659. | 3.3 | 38 |
| 27 | Combustion synthesized macroporous structure MFe 2 O 4 (M= Zn, Co) as anode materials with excellent electrochemical performance for lithium ion batteries. Journal of Alloys and Compounds, 2017, 699, 401-407. | 5.5 | 38 |
| 28 | Altering the Static Dipole on Surfaces through Chemistry: Molecular Films of Zwitterionic Quinonoids. Journal of the American Chemical Society, 2012, 134, 8494-8506. | 13.7 | 37 |
| 29 | The role of the interface in the electronic structure of adsorbed metal(II) (Co, Ni, Cu) phthalocyanines. Journal of Materials Chemistry, 2009, 19, 2172. | 6.7 | 36 |
| 30 | Facile design of ultrafine CuFe2O4 nanocrystallines coupled porous carbon nanowires: Highly effective electrocatalysts for hydrogen peroxide reduction and the oxygen evolution reaction. Journal of Alloys and Compounds, 2019, 809, 151766. | 5.5 | 36 |
| 31 | An investigation on the kinetics of direct carbon solid oxide fuel cells. Journal of Solid State Electrochemistry, 2016, 20, 2207-2216. | 2.5 | 34 |
| 32 | Valence holes observed in nanodiamonds dispersed in water. Nanoscale, 2015, 7, 2987-2991. | 5.6 | 33 |
| 33 | The interface bonding and orientation of a quinonoid zwitterion. Physical Chemistry Chemical Physics, 2010, 12, 10329. | 2.8 | 30 |
| 34 | Evolution of Oxygen–Metal Electron Transfer and Metal Electronic States During Manganese Oxide Catalyzed Water Oxidation Revealed with Inâ€Situ Soft Xâ€Ray Spectroscopy. Angewandte Chemie, 2019, 131, 3464-3470. | 2.0 | 28 |
| 35 | Comparison of the electronic structure of two polymers with strong dipole ordering. Journal of Physics Condensed Matter, 2006, 18, L155-L161. | 1.8 | 26 |
| 36 | The Electronic Structure and Secondary Pyroelectric Properties of Lithium Tetraborate. Materials, 2010, 3, 4550-4579. | 2.9 | 24 |

| # | Article | IF | CITATIONS |
|----|--|------|-----------|
| 37 | New insights into carbon deposition mechanism of nickel/yttrium-stabilized zirconia cermet from methane by in situ investigation. Applied Energy, 2019, 256, 113910. | 10.1 | 24 |
| 38 | Effect of pre-calcined ceramic powders at different temperatures on Ni-YSZ anode-supported SOFC cell/stack by low pressure injection molding. Ceramics International, 2019, 45, 20066-20072. | 4.8 | 23 |
| 39 | Stable Acidic Water Oxidation with a Cobalt–Iron–Lead Oxide Catalyst Operating via a Cobaltâ€5elective Selfâ€Healing Mechanism. Angewandte Chemie - International Edition, 2021, 60, 15821-15826. | 13.8 | 23 |
| 40 | Characterization of the soft X-ray spectrometer PEAXIS at BESSYâ€II. Journal of Synchrotron Radiation, 2020, 27, 238-249. | 2.4 | 23 |
| 41 | Co-precipitation synthesis of alumina doped yttria stabilized zirconia. Journal of Alloys and Compounds, 2018, 731, 1080-1088. | 5.5 | 22 |
| 42 | Undistorted X-ray Absorption Spectroscopy Using s-Core-Orbital Emissions. Journal of Physical Chemistry A, 2016, 120, 2808-2814. | 2.5 | 21 |
| 43 | TiO2–MoS2 hybrid nano composites with 3D network architecture as binder-free flexible electrodes for lithium ion batteries. Journal of Materials Science: Materials in Electronics, 2017, 28, 9519-9527. | 2.2 | 21 |
| 44 | Selective nanoshaving of self-assembled monolayers of 2-(4-pyridylethyl)triethoxysilane. Materials Letters, 2009, 63, 961-964. | 2.6 | 20 |
| 45 | On the Origin of the Improvement of Electrodeposited MnOxFilms in Water Oxidation Catalysis Induced by Heat Treatment. ChemSusChem, 2015, 8, 1980-1985. | 6.8 | 20 |
| 46 | Coverage―and Temperatureâ€Dependent Metalation and Dehydrogenation of Tetraphenylporphyrin on Cu(111). Chemistry - A European Journal, 2014, 20, 8948-8953. | 3.3 | 19 |
| 47 | Coordination Reactions and Layer Exchange Processes at a Buried Metal–Organic Interface. Journal of Physical Chemistry C, 2014, 118, 8501-8507. | 3.1 | 19 |
| 48 | Crystalline Ice Grown on the Surface of the Ferroelectric Polymer Poly(vinylidene fluoride) (70%) and Trifluoroethylene (30%). Journal of the American Chemical Society, 2005, 127, 17261-17265. | 13.7 | 18 |
| 49 | The off-axis pyroelectric effect observed for lithium tetraborate. Physics Letters, Section A: General, Atomic and Solid State Physics, 2010, 374, 891-895. | 2.1 | 18 |
| 50 | A Microtubular Direct Carbon Solid Oxide Fuel Cell Operated on the Biochar Derived from Pepper Straw. Energy Technology, 2020, 8, 1901077. | 3.8 | 18 |
| 51 | Adsorbate/absorbate interactions with organic ferroelectric polymers. Journal of Electron Spectroscopy and Related Phenomena, 2009, 174, 10-21. | 1.7 | 16 |
| 52 | Weak screening of a large dipolar molecule adsorbed on graphene. Carbon, 2012, 50, 1981-1986. | 10.3 | 16 |
| 53 | Electronic Structure of Hemin in Solution Studied by Resonant X-ray Emission Spectroscopy and Electronic Structure Calculations. Journal of Physical Chemistry B, 2014, 118, 9938-9943. | 2.6 | 16 |
| 54 | Introducing Ionic-Current Detection for X-ray Absorption Spectroscopy in Liquid Cells. Journal of Physical Chemistry Letters, 2017, 8, 2087-2092. | 4.6 | 16 |

| # | Article | IF | CITATIONS |
|----|--|-----|-----------|
| 55 | Facile synthesis of cobalt nanoparticles encapsulated in nitrogen-doped carbon nanotubes for use as a highly efficient bifunctional catalyst in rechargeable Zn-Air batteries. Journal of Alloys and Compounds, 2020, 842, 155791. | 5.5 | 16 |
| 56 | A novel Chinese parasol leaf biochar fuelled direct carbon solid oxide fuel cell for high performance electricity generation. International Journal of Hydrogen Energy, 2022, 47, 1172-1182. | 7.1 | 16 |
| 57 | Different approaches to adjusting band offsets at intermolecular interfaces. Applied Surface Science, 2008, 254, 4238-4244. | 6.1 | 15 |
| 58 | Chemical Speciation and Bond Lengths of Organic Solutes by Coreâ€Level Spectroscopy: pH and Solvent Influence on <i>p</i> â€Aminobenzoic Acid. Chemistry - A European Journal, 2015, 21, 7256-7263. | 3.3 | 15 |
| 59 | In-Situ X-ray Spectroscopy of the Electric Double Layer around TiO ₂ Nanoparticles Dispersed in Aqueous Solution: Implications for H ₂ Generation. ACS Applied Nano Materials, 2020, 3, 264-273. | 5.0 | 15 |
| 60 | Chemical bonding in aqueous hexacyano cobaltate from photon- and electron-detection perspectives. Scientific Reports, 2017, 7, 40811. | 3.3 | 14 |
| 61 | A Fast and Effective Sensitivity Calculation Method for Circuit Input Vectors. IEEE Transactions on Reliability, 2019, 68, 938-953. | 4.6 | 14 |
| 62 | Performance improvement of a direct carbon solid oxide fuel cell via strontium-catalyzed carbon gasification. International Journal of Hydrogen Energy, 2020, 45, 23368-23377. | 7.1 | 14 |
| 63 | The surface core level shift for lithium at the surface of lithium borate. Physica B: Condensed Matter, 2010, 405, 461-464. | 2.7 | 13 |
| 64 | Uncovering the Charge Transfer between Carbon Dots and Water by In Situ Soft X-ray Absorption Spectroscopy. Journal of Physical Chemistry Letters, 2019, 10, 3843-3848. | 4.6 | 13 |
| 65 | Nafionâ€Induced Reduction of Manganese and its Impact on the Electrocatalytic Properties of a Highly Active MnFeNi Oxide for Bifunctional Oxygen Conversion**. ChemElectroChem, 2021, 8, 2979-2983. | 3.4 | 13 |
| 66 | Co(iii) protoporphyrin IX chloride in solution: spin-state and metal coordination revealed from resonant inelastic X-ray scattering and electronic structure calculations. Physical Chemistry Chemical Physics, 2015, 17, 3409-3414. | 2.8 | 12 |
| 67 | Circuit reliability estimation based on an iterative PTM model with hybrid coding. Microelectronics Journal, 2016, 52, 117-123. | 2.0 | 12 |
| 68 | Local Energy Gap Opening Induced by Hemin Dimerization in Aqueous Solution. Journal of Physical Chemistry B, 2015, 119, 3058-3062. | 2.6 | 11 |
| 69 | Xâ€Ray Absorption Spectroscopy of TiO ₂ Nanoparticles in Water Using a Holey Membraneâ€Based Flow Cell. Advanced Materials Interfaces, 2017, 4, 1700755. | 3.7 | 11 |
| 70 | Generalized Synchronization Between Chen System and Rucklidge System. IEEE Access, 2019, 7, 8519-8526. | 4.2 | 11 |
| 71 | The Electronic Structures of Co and Ni Tetraazaannulenes. Journal of Physical Chemistry B, 2006, 110, 26180-26184. | 2.6 | 10 |
| 72 | Influence of the Outer Ligands on Metal-to-Ligand Charge Transfer in Solvated Manganese Porphyrins. Inorganic Chemistry, 2016, 55, 22-28. | 4.0 | 10 |

| # | Article | IF | CITATIONS |
|----|--|-----|-----------|
| 73 | Bulk-Sensitive Detection of the Total Ion Yield for X-ray Absorption Spectroscopy in Liquid Cells. Journal of Physical Chemistry Letters, 2017, 8, 5136-5140. | 4.6 | 10 |
| 74 | Innovative Savonius rotors evolved by genetic algorithm based on 2D-DCT encoding. Soft Computing, 2018, 22, 8001-8010. | 3.6 | 10 |
| 75 | Surface charging at the (100) surface of Cu doped and undoped Li2B4O7. Applied Surface Science, 2011, 257, 3399-3403. | 6.1 | 9 |
| 76 | Intermolecular bonding of hemin in solution and in solid state probed by N K-edge X-ray spectroscopies. Physical Chemistry Chemical Physics, 2015, 17, 29000-29006. | 2.8 | 9 |
| 77 | Blockchain Architecture Reliability-Based Measurement for Circuit Unit Importance. IEEE Access, 2018, 6, 15326-15334. | 4.2 | 9 |
| 78 | Improving Robustness of Interdependent Networks by Reducing Key Unbalanced Dependency Links. IEEE Transactions on Circuits and Systems II: Express Briefs, 2020, 67, 3187-3191. | 3.0 | 9 |
| 79 | BM-RCGL: Benchmarking Approach for Localization of Reliability-Critical Gates in Combinational Logic Blocks. IEEE Transactions on Computers, 2022, 71, 1063-1076. | 3.4 | 9 |
| 80 | A Method of Gate-Level Circuit Reliability Estimation Based on Iterative PTM Model. , 2011, , . | | 8 |
| 81 | A Locating Method for Reliability-Critical Gates with a Parallel-Structured Genetic Algorithm. Journal of Computer Science and Technology, 2019, 34, 1136-1151. | 1.5 | 8 |
| 82 | Highly efficient utilization of industrial barium slag for carbon gasification in direct carbon solid oxide fuel cells. International Journal of Hydrogen Energy, 2021, 46, 37029-37038. | 7.1 | 8 |
| 83 | Assistance of the Iron Porphyrin Ligands to the Binding Interaction between the Fe Center and Small Molecules in Solution. Journal of Physical Chemistry B, 2014, 118, 9371-9377. | 2.6 | 7 |
| 84 | Enhancing Catalytic Activity by Narrowing Local Energy Gaps—Xâ€Ray Studies of a Manganese Water Oxidation Catalyst. ChemSusChem, 2015, 8, 872-877. | 6.8 | 7 |
| 85 | Link prediction based on local major path degree. Modern Physics Letters B, 2018, 32, 1850348. | 1.9 | 7 |
| 86 | Comparative Study of Yttria-Stabilized Zirconia Synthesis by Co-Precipitation and Solvothermal Methods. Jom, 2019, 71, 3806-3813. | 1.9 | 7 |
| 87 | Investigation on the formation mechanism of twinned crystals of hypoxanthine-doped beta-phase anhydrous guanine microplatelets. CrystEngComm, 2021, 23, 3444-3452. | 2.6 | 7 |
| 88 | Uniform non-Bernoulli sequences oriented locating method for reliability-critical gates. Tsinghua Science and Technology, 2021, 26, 24-35. | 6.1 | 7 |
| 89 | Analysis of the Electronic Structure of Aqueous Urea and Its Derivatives: A Systematic Soft Xâ€Ray–TDâ€DFT Approach. Chemistry - A European Journal, 2016, 22, 12040-12049. | 3.3 | 6 |
| 90 | A Novel Trust Evaluation Method for Logic Circuits in IoT Applications Based on the E-PTM Model. IEEE Access, 2018, 6, 35683-35696. | 4.2 | 6 |

| # | Article | IF | CITATIONS |
|-----|--|--------------------|--------------------|
| 91 | Identifying Reliability-Critical Primary Inputs of Combinational Circuits Based on the Model of Gate-Sensitive Attributes. IEEE Transactions on Computer-Aided Design of Integrated Circuits and Systems, 2022, 41, 4708-4720. | 2.7 | 6 |
| 92 | Insight into pHâ€Dependent Formation of Manganese Oxide Phases in Electrodeposited Catalytic Films Probed by Soft Xâ€Ray Absorption Spectroscopy. ChemPlusChem, 2018, 83, 721-727. | 2.8 | 5 |
| 93 | Circuit reliability prediction based on deep autoencoder network. Neurocomputing, 2019, 370, 140-154. | 5.9 | 5 |
| 94 | Sex-related Difference in Mental Rotation Performance is Mediated by the special Functional Connectivity Between the Default Mode and Salience Networks. Neuroscience, 2021, 478, 65-74. | 2.3 | 5 |
| 95 | Flower-like three-dimensional bifunctional cathode catalyst for high-performance Li–O2 batteries: ZIF-67@3D-N/rGO. Ceramics International, 2022, 48, 5601-5608. | 4.8 | 5 |
| 96 | Electronic structure evidence for allâ€ŧrans poly(methylvinylidene cyanide). Polymer Engineering and Science, 2008, 48, 1649-1654. | 3.1 | 4 |
| 97 | Haloform adsorption on crystalline copolymer films of vinylidene fluoride with trifluoroethylene. Surface Science, 2009, 603, 513-517. | 1.9 | 4 |
| 98 | Low Remanent Polarization for High Energy Density by Poly(vinylidene) Tj ETQq0 0 0 rgBT /Overlock 10 Tf 50 46 Materials, 2019, 48, 8172-8180. | 7 Td (fluor 2.2 | ide-co-chloro 4 |
| 99 | Blends based P(VDF-CTFE) with quenching in ice water and PLZST modification with high energy storage performance. Polymer, 2020, 202, 122727. | 3.8 | 4 |
| 100 | Franckâ^'Condon Coupling in Anthracene Isomer Self-Assembled Layers and Symmetry Effects on the High Resolution Ultraviolet Photoemission Spectra. Journal of Physical Chemistry C, 2010, 114, 1015-1018. | 3.1 | 3 |
| 101 | Stable Acidic Water Oxidation with a Cobalt–Iron–Lead Oxide Catalyst Operating via a Cobaltâ€Selective Selfâ€Healing Mechanism. Angewandte Chemie, 2021, 133, 15955-15960. | 2.0 | 3 |
| 102 | Structural and functional biomarkers of the insula subregions predict sex differences in aggression subscales. Human Brain Mapping, 2022, 43, 2923-2935. | 3.6 | 3 |
| 103 | Electrochemical Performance of Cone-Shaped Tubular Anode Supported Solid Oxide Fuel Cells Fabricated by Low-Pressure Injection Moulding Technique. ECS Transactions, 2011, 35, 609-614. | 0.5 | 2 |
| 104 | Multiscale Photo-Based In-Situ and Operando Spectroscopies in Time and Energy Landscapes. Synchrotron Radiation News, 2017, 30, 14-19. | 0.8 | 2 |
| 105 | Laplacian Centrality Peaks Clustering Based on Potential Entropy. IEEE Access, 2018, 6, 55462-55472. | 4.2 | 1 |
| 106 | Thermal-aware SoC Test Scheduling with Voltage/Frequency Scaling and Test Partition. Journal of Electronic Testing: Theory and Applications (JETTA), 2018, 34, 447-460. | 1.2 | 1 |
| 107 | Accelerating stochasticâ€based reliability estimation for combinational circuits at RTL using GPU parallel computing. International Journal of Intelligent Systems, 2022, 37, 8309-8326. | 5.7 | 1 |
| 108 | A Method of Gate-level Circuit Yield Calculation Based on PTM. Procedia Computer Science, 2017, 107, 674-684. | 2.0 | 0 |

| # / | Article | IF | CITATIONS |
|--------------|---|----|-----------|
| 109 <i>k</i> | A Stochastic-Based Reliability Calculation Method for RTL Circuits. , 2020, , . | | 0 |